Title	Electron-phonon coupling and electronic thermoelectric properties of n-type PbTe driven near the soft-mode phase transition via lattice expansion
Author(s)	Cao, Jiang; Dangić, Đorđe; Querales-Flores, José D.; Fahy, Stephen B.; Savić, Ivana
Publication date	2021-07-12
Original citation	Cao, J., Dangić, Đ., Querales-Flores, J. D., Fahy, S. and Savić, I. (2021) 'Electron-phonon coupling and electronic thermoelectric properties of n-type PbTe driven near the soft-mode phase transition via lattice expansion', Physical Review B, 104, 045202 (8pp). doi: 10.1103/PhysRevB.104.045202
Type of publication	Article (peer-reviewed)
Link to publisher's version	http://dx.doi.org/10.1103/PhysRevB.104.045202 Access to the full text of the published version may require a subscription.
Rights	© 2021, American Physical Society. All rights reserved.
Item downloaded from	http://hdl.handle.net/10468/11584

University College Cork, Ireland
Coláiste na hOllscoile Corcaigh

Electron-phonon coupling and electronic thermoelectric properties of *n*-type PbTe driven near the soft-mode phase transition via lattice expansion

Jiang Cao [1,2,*] Đorđe Dangić [2,3] José D. Querales-Flores [2] Stephen Fahy,[2,3] and Ivana Savić[2,†]

[1]*School of Electronic and Optical Engineering, Nanjing University of Science and Technology, Nanjing 210094, China*
[2]*Tyndall National Institute, Dyke Parade, Cork T12R5CP, Ireland*
[3]*Department of Physics, University College Cork, College Road, Cork T12K8AF, Ireland*

IV–VI materials are some of the most efficient bulk thermoelectric materials due to their proximity to soft-mode phase transitions, which leads to low lattice thermal conductivity. It has been shown that the lattice thermal conductivity of PbTe can be considerably reduced by bringing PbTe closer to the phase transition, e.g., via lattice expansion. However, the effect of soft phonon modes on the electronic thermoelectric properties of such a system remains unknown. Using first-principles calculations, we show that the soft zone-center transverse optical phonons do not deteriorate the electronic thermoelectric properties of PbTe driven closer to the phase transition via lattice expansion due to external stress, and thus they enhance the thermoelectric figure of merit. We find that the optical deformation potentials change very weakly as the proximity to the phase transition increases, but the population and scattering phase space of soft phonon modes increase. Nevertheless, scattering between electronic states near the band edge and soft optical phonons remains relatively weak even very near the phase transition.

I. INTRODUCTION

The metric by which the performance of a thermoelectric material is measured is the thermoelectric figure of merit, $ZT = (\sigma S^2 T)/(\kappa_e + \kappa_L)$, where S is the Seebeck coefficient, σ is the electrical conductivity, T is the temperature, and κ_e and κ_L are the electronic and lattice contribution to thermal conductivity, respectively [1–3]. Achieving high ZT values requires a high power factor (PF $= S^2\sigma$) and low κ_e and κ_L. The electronic transport properties S, σ, and κ_e are correlated, while κ_L is to some degree independent from the electronic properties in semiconductors.

Reducing κ_L without changing electronic transport properties in a material is a frequently used approach for improving ZT, known as the "phonon-glass–electron-crystal" approach [4,5]. It has been recently recognized that the proximity to soft-mode phase transitions is one of the key ingredients in suppressing the lattice thermal conductivity of IV–VI thermoelectric materials [6–12]. Bringing SnSe near its soft-mode phase transition via temperature has been shown to enhance anharmonicity and reduce κ_L [10,13–15]. Similar effects have also been predicted for PbTe driven to a different type of the soft-mode phase transition via strain or alloying [11,12,16,17]. An important open question is whether soft phonon modes can lead to strong electron-phonon (e-ph) scattering and actually reduce the PF, thus competing with the benefit of lowering κ_L for improved thermoelectric performance.

We have recently shown using first-principles calculations that soft phonon modes in PbTe interact weakly with the electronic states relevant for thermoelectric transport [18,19]. Such weak e-ph scattering was partially attributed to the symmetry-forbidden conduction band intravalley scattering (by the Γ-point phonons). However, this symmetry restriction at *L* (the band minimum) becomes insufficient in explaining the strength of e-ph coupling as the material approaches the soft-mode phase transition. In this case, the soft-mode frequency becomes nearly zero, and the soft modes exhibit almost an acousticlike dispersion relation near the Brillouin zone center. As the proximity to the soft-mode phase transition increases, scattering due to soft optical phonon modes becomes increasingly like that due to acoustic phonons, which is also forbidden at the band minimum *L* but nevertheless relatively strong for carriers near *L*, which are active in thermoelectric transport in PbTe. Moreover, the optical deformation potentials are much larger than those of acoustic phonons in equilibrium PbTe [18], which could make electron–soft-mode scattering significantly stronger closer to the phase transition if the optical deformation potentials are not significantly reduced. As PbTe approaches the phase transition, the decreasing transverse optical (TO) phonon frequency will significantly increase the TO phonon population and the e-ph scattering phase space, thus increasing the e-ph scattering due to the soft modes. For example, recent first-principles calculations in $SrTiO_3$ have revealed that soft phonon modes become the dominant e-ph scattering channel near the Curie temperature [20]. Whether soft modes become the dominant electronic scattering channel in a particular material depends on the exact magnitude of deformation potentials close to the phase transition, which cannot be known

*jiang.cao@njust.edu.cn
†ivana.savic@tyndall.ie

a priori from the symmetry analysis alone and calls for first-principles calculations.

In this paper, we show from first-principles calculations that driving *n*-type PbTe close to its soft-mode phase transition via lattice expansion due to external stress does not degrade the electronic transport properties. We find that optical deformation potentials do not change much with strain. Since the soft-mode populations and scattering phase space increase as PbTe is driven closer to the phase transition, soft TO modes interact more strongly with the electronic states determining thermoelectric transport. However, soft TO modes remain a relatively weak e-ph scattering channel compared with long-range polar longitudinal optical (LO) phonon modes. Consequently, increasing the proximity to the soft-TO-mode phase transition via lattice expansion does not have a detrimental effect on the electronic thermoelectric properties of PbTe. This result, together with the earlier predictions of a significant κ_L decrease in PbTe driven closer to the phase transitions (roughly by a factor of 2) [11], indicates a potential considerable increase in *ZT* near the phase transition.

II. METHOD

We employed the thermoelectric transport model developed in our previous work and tested for PbTe against many experiments [18,19,21]. We calculated all the parameters of the model from first principles, thus relying on no free parameters. The accuracy of our transport model in calculating the e-ph relaxation times using the density functional theory (DFT) electronic band structure is similar to that of the state-of-the-art electron-phonon coupling using Wannier functions (EPW) code [22], as shown in Sec. III and Refs. [18,19]. The results of our model are directly comparable with those of the EPW code when we use parametrized electronic and phonon band structures obtained with DFT and density functional perturbation theory (DFPT) [23,24], respectively, and the QUANTUM ESPRESSO package [25,26]. However, unlike the current version of the EPW code, our transport model allows using a more accurate electronic band structure than that computed with DFT and accounting for its temperature dependence, as described in the following.

In order to get the electronic band structure with an accurate band gap and the correct character of conduction and valence band edge states, we used the screened Heyd-Scuseria-Ernzerhof (HSE03) hybrid functional including spin-orbit coupling (SOC) [27,28] and the Vienna *ab initio* simulation package (VASP) [29]. The basis set for the one-electron wave functions was constructed with the projector augmented wave method [30]. In PbTe, the direct band gap is located at the L points in the Brillouin zone (BZ), and only the electronic states in the vicinity of the L points contribute to electronic transport [18]. The HSE03 lowest conduction band was fitted to the two-band Kane model near the L points, using the parallel and perpendicular effective masses $m^*_{\perp,\parallel}$ and the nonparabolic parameter set to the inverse of the band gap $1/E_g$ [18].

In our electronic transport model, we also accounted for the temperature dependence of the band gap due to e-ph interactions using the nonadiabatic Allen-Heine-Cardona (AHC) formalism [31–33] and DFPT [23,24], as implemented in

ABINIT [34]. We calculated $\partial E_g/\partial T = 2.98 \times 10^{-4}$ eV/K [35]. The effective masses are taken to depend on temperature as $m^*_{\perp,\parallel}(T)/m^*_{\perp,\parallel}(0\text{ K}) = E_g(T)/E_g(0\text{ K})$ according to the two-band Kane model [36]. We note that the thermal expansion contribution to $\partial E_g/\partial T$ is excluded in this paper since we explicitly investigate the effect of lattice expansion on thermoelectric transport.

To calculate phonon band structures and e-ph matrix elements, we adopted the DFPT framework as implemented in the QUANTUM ESPRESSO package [25,26], using the local density approximation (LDA) excluding SOC with the Hartwigsen-Goedecker-Hutter (HGH) norm-conserving pseudopotentials. In our previous work, we verified that the LDA without SOC gives very similar e-ph matrix elements compared with the HSE03 with SOC [37]. For the LDA with SOC, the e-ph matrix elements are ill defined, because the conduction band minimum and valence band maximum states are interchanged and mix heavily, forming an incorrect "negative band gap" [37]. In our DFPT calculations of e-ph matrix elements, we used $12 \times 12 \times 12$ and $6 \times 6 \times 6$ reciprocal space grids for electronic and phonon states, respectively, and the cutoff energy was set to 70 Ry. The e-ph matrix elements were then interpolated on finer $40 \times 40 \times 40$ **k** and **q** grids using the Wannier functions method [38] and the EPW code [22]. Fourteen Wannier orbitals were constructed from Bloch states on a $12 \times 12 \times 12$ **k**-point grid using the WANNIER90 code [39].

In PbTe, scattering at the L points caused by the X-point phonons is forbidden by symmetry [18]. Moreover, X-point phonon frequencies remain nonzero throughout the range of lattice and temperature parameters of our study. As a result, only phonons near the zone center contribute to electronic scattering processes in *n*-type PbTe in our model, which is verified against rigorous EPW calculations (see Sec. III). We parametrized nonpolar and polar Fröhlich e-ph scattering mechanisms using the approach developed in our previous work [18,37]. Acoustic and optical deformation potentials were calculated by fitting the corresponding e-ph matrix elements with the deformation potential Hamiltonian in the long-wavelength limit along five high-symmetry directions of **q** in a cubic crystal [37,40,41]. Ionized-impurity scattering induced by dopant atoms was accounted for using the Brooks-Herring model [42] with Thomas-Fermi screening. Elastic and dielectric constants for the polar Fröhlich perturbation Hamiltonian were obtained from DFPT.

Electronic transport quantities were calculated using the Boltzmann transport theory within the transport (momentum) relaxation time approximation as

$$\begin{cases} \sigma & = L_0 \\ S & = -L_1/(eTL_0) \\ \kappa_0 & = L_2/(e^2T), \end{cases} \tag{1}$$

where σ is the electrical conductivity tensor, S is the Seebeck coefficient tensor, κ_0 is the thermal conductivity tensor defined when the electric field across the material is zero, and e is the electron charge value. The transport kernel functions for the conduction band are defined by

$$L_\alpha = \int_{\text{BZ}} \frac{e^2 d\boldsymbol{k}}{4\pi^3} \left(-\frac{\partial f}{\partial E}\right) \tau_{\boldsymbol{k},\text{tot}} \bar{v}_{\boldsymbol{k}}^2 (E_{\boldsymbol{k}} - E_F)^\alpha, \tag{2}$$
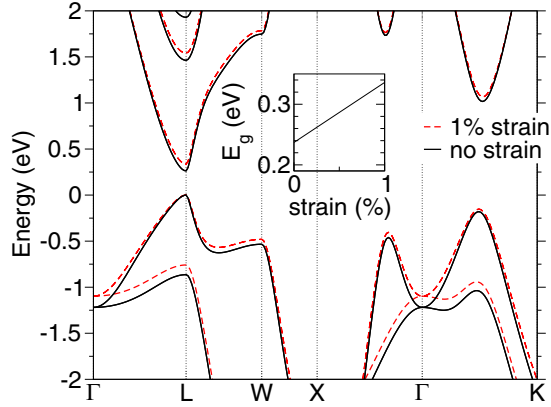
FIG. 1. Electronic band structure at 0 K for PbTe with the equilibrium lattice constant (solid black lines) and the 1% larger lattice constant (dashed red lines). The inset shows direct band gap vs strain.

where E_k is the energy of the conduction band state with the crystal momentum $\boldsymbol{k}$, $\bar{v}_k = [\sum_i (v_k^i)^2/3]^{1/2}$ is the group velocity averaged over directions, i denotes the Cartesian directions, f is the Fermi-Dirac distribution function, E_F is the Fermi level, and $\tau_{k,\text{tot}}$ is the total transport relaxation time of all scattering channels [18].

III. RESULTS AND DISCUSSION

A. Electronic band structure

PbTe has the conduction band minima (CBM) and the valence band maxima (VBM) located at the four L points in the BZ. In Fig. 1, we plot the electronic band structure calculated using the HSE03 hybrid functional for PbTe with the equilibrium and 1% expanded lattice constants ($a_{\text{latt}} = a_0$ and $a_{\text{latt}} = 1.01a_0$, respectively). Most importantly, strain has a fairly weak effect on the electronic band structure close to the Fermi energy. The direct band gap at the L points (E_g) is increased from 0.238 to 0.336 eV by applying 1% of strain, as shown in the inset of Fig. 1. The conduction and valence band effective masses also increase with the band gap. We can accurately fit the HSE03 conduction band within 0.5 eV from the CBM using the Kane model if we use $1/E_g$ as the nonparabolic parameter of the Kane model and the effective masses calculated using the LDA without SOC given in Table I.

B. Transverse optical mode softening

PbTe crystallizes in the rocksalt structure up to the melting temperature of ~1200 K [43]. Nevertheless, it is energetically close to the phase transition to the rhombohedral phase, characterized by the internal atomic displacement of Te, which corresponds to a frozen-in atomic motion of the zone-center TO mode along the [111] direction in the rocksalt structure. As a result, the TO phonon modes near the zone center in PbTe are very soft [6,44]; see the black solid lines in Fig. 2. If the lattice is expanded via external stress, the frequencies of the soft TO modes near the Γ point further decrease (the red solid lines in Fig. 2), since the potential energy surface flattens as PbTe approaches the soft-mode phase transition. To gain

TABLE I. Parameters used in the calculation of electronic transport quantities and computed from first principles for n-type PbTe with the equilibrium lattice constant (no strain, $\eta = 0$) and the lattice constant expanded by 1% ($\eta = 1\%$ of strain): lattice constant in the local density approximation a_{latt}, acoustic deformation potentials Ξ_d^{ac} and Ξ_u^{ac}, optical deformation potentials Ξ_d^{opt} and Ξ_u^{opt}, optical phonon frequencies $\omega_\Gamma^{\text{LO}}$ and $\omega_\Gamma^{\text{TO}}$, TO phonon dispersion parameter q_0, high-frequency and static dielectric constants ϵ_∞ and ϵ_s, elastic constants c_{11}, c_{12}, and c_{44}, direct band gap from the hybrid functional calculations E_g^{HSE}, and parallel and perpendicular effective masses at the conduction band minimum $m_\parallel^*$ and $m_\perp^*$.

η	0	1%
a_{latt} (Å)	6.348	6.411
Ξ_d^{ac} (eV)	0.37	0.36
Ξ_u^{ac} (eV)	7.03	6.48
Ξ_d^{opt} (eV)	19.09	19.56
Ξ_u^{opt} (eV)	-34.24	-34.79
$\omega_\Gamma^{\text{LO}}$ (THz)	3.2	3.1
$\omega_\Gamma^{\text{TO}}$ (THz)	0.95	0.15
q_0 (nm^{-1})	1.61	0.254
ϵ_∞	34.85	33.59
ϵ_s	356.8	14346.0
c_{11} (GPa)	136.4	120.6
c_{12} (GPa)	3.8	4.5
c_{44} (GPa)	17.1	17.0
E_g^{HSE} (eV)	0.238	0.336
$m_\parallel^*/m_0$	0.216	0.241
$m_\perp^*/m_0$	0.037	0.043

more insight into the TO mode behavior near the soft-mode phase transition, Fig. 3 shows the TO mode frequency at the Γ point, $\omega_{\text{TO}}^\Gamma$, as a function of the lattice constant and the corresponding strain. $\omega_{\text{TO}}^\Gamma$ can be fitted to $\omega_{\text{TO}}^\Gamma = \alpha\sqrt{a_c - a_{\text{latt}}}$, with $\alpha = 3.672\,46$ THz Å$^{-0.5}$ and $a_c = 6.413\,38$ Å, shown by the black dashed line in Fig. 3. LO and acoustic modes are much
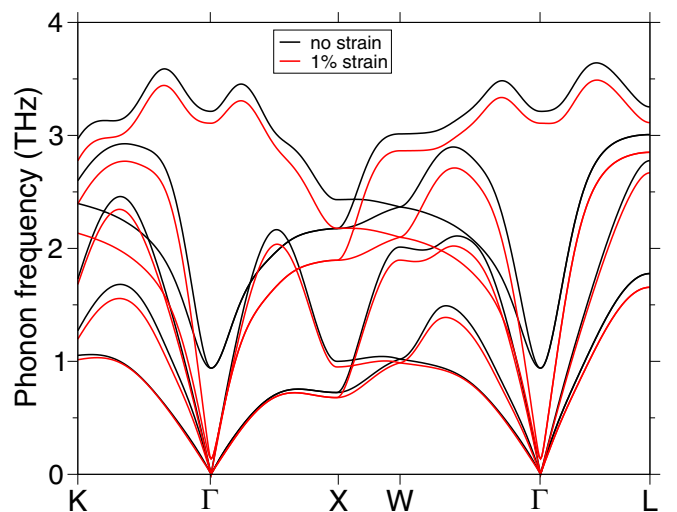

FIG. 2. Phonon dispersion for PbTe with the equilibrium lattice constant (black lines) and the 1% larger lattice constant (red lines), obtained using density functional perturbation theory (DFPT).
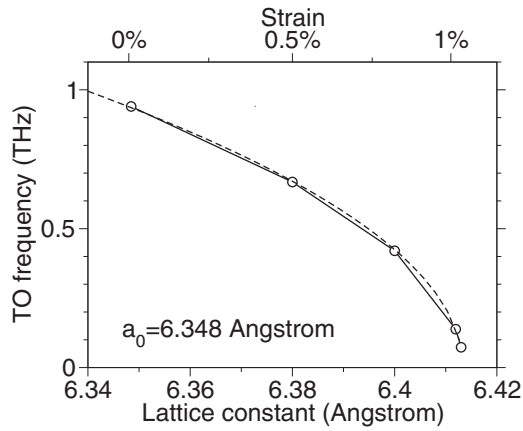
FIG. 3. Frequency of transverse optical (TO) modes at the zone center for PbTe vs lattice constant and strain, calculated using density functional perturbation theory (DFPT). The dashed black line represents a fit to the DFPT results.

less sensitive to changes in the lattice constant compared with soft TO modes (Fig. 2).

C. Electron-phonon interaction

To accurately describe the e-ph interaction in *n*-type PbTe driven close to the phase transition via lattice expansion, we calculated all the relevant quantities [18] from first principles for the equilibrium and 1% expanded lattice constants, as reported in Table I. The elastic constants do not vary considerably with strain, reflecting the same trend seen for acoustic phonon branches, as well as the LO phonon frequency (Fig. 2). The only phonon quantities that change significantly while varying the amount of strain are the TO phonon frequency at Γ, ω_{TO}^{Γ}, and the TO dispersion in the vicinity of Γ (Fig. 2). We note that the TO dispersion near Γ was modeled as $\omega_{TO}^{q} = \omega_{TO}^{\Gamma}\sqrt{1 + |q|^2/q_0^2}$, which transforms smoothly from equilibrium to 1% strain as q_0 decreases with ω_{TO}^{Γ}; see Table I.

The high-frequency dielectric constant ϵ_{∞} does not change much with lattice expansion since the electronic band structure is not substantially modified. However, the static dielectric constant ϵ_s diverges towards the phase transition as a result of the Lyddane-Sachs-Teller (LST) relation [45]: $(\omega_{LO}^{\Gamma}/\omega_{TO}^{\Gamma})^2 = \epsilon_s/\epsilon_{\infty}$.

Since the electronic band structure and acoustic phonons of PbTe depend weakly on strain, the acoustic deformation potentials do not change much with strain; see Table I. Surprisingly, despite the fact that ω_{TO} varies significantly with strain, the optical deformation potentials are relatively insensitive to it. We emphasize that it is impossible to *a priori* know the variation of deformation potentials with strain without carrying out these first-principles calculations. In the following calculations, we will only update the values of ω_{TO}^{Γ}, q_0, and ϵ_s as a function of strain, as well as the parameters of the electronic band structure, i.e., the band gap and the effective masses.

Next we compute the e-ph scattering rates of PbTe using our model and compare them with those obtained using the
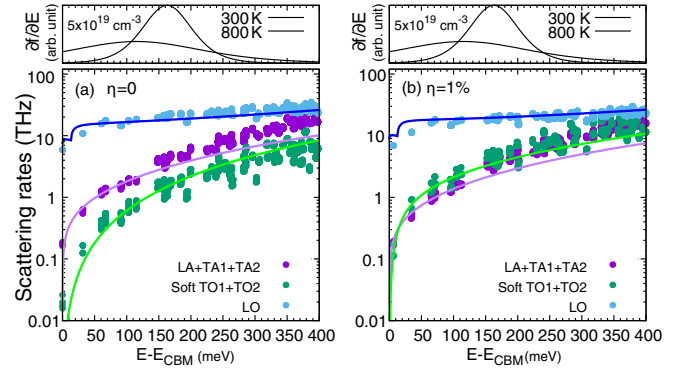

FIG. 4. Electron-phonon scattering rates at 300 K resolved by phonon mode as a function of electronic energy for PbTe with (a) no applied strain ($\eta = 0$) and (b) 1% of strain ($\eta = 1\%$). The energy derivative of the Fermi distribution function for the doping concentration of 5×10^{19} cm^{-3} is also plotted for 300 and 800 K. The zero of the energy axis is the conduction band minimum. LA, longitudinal acoustic; TA, transverse acoustic.

EPW code, which makes no assumptions about the *k*- and *q*-point dependence of e-ph matrix elements and their changes with strain [22]. In the EPW calculations, we used $40 \times 40 \times 40$ *k*- and *q*-point grids, and the Gaussian broadening parameter was set to 40 meV. Figure 4 shows the mode-resolved e-ph scattering rates for *n*-type PbTe under different strain conditions at 300 K, calculated using our model and the EPW code. We note that the model is in very good agreement with the EPW results for all the phonon modes and for different strain values. This finding highlights the accuracy of our model and further justifies our assumption of keeping the acoustic and optical deformation potentials, ϵ_{∞}, and the elastic constants constant.

Scattering due to LO phonons is the strongest e-ph scattering mechanism in equilibrium PbTe, while scattering due to soft TO phonons is the weakest [Fig. 4(a)]. In our previous work, we found that the latter effect partly arises because the electron–TO-mode matrix element is zero by symmetry for the conduction (and valence) band states at L and the zone-center TO modes in the rocksalt structure [18]. Similarly, the intervalley L-L scattering caused by the X-point phonons also vanishes [18].

In spite of this symmetry restriction, it is *a priori* unclear whether the strength of electron–TO-phonon scattering will increase as PbTe approaches the phase transition due to lattice expansion. Extremely soft optical phonons behave almost like acoustic phonons, whose scattering at the zone center is also forbidden. Moreover, uniaxial optical deformation potentials are significantly larger than those of acoustic phonons (see Table I), and scattering rates are proportional to their square. This suggests that scattering due to soft optical modes may become stronger near the phase transition.

We find that the strength of electron–TO-phonon scattering indeed increases as PbTe approaches the phase transition, as shown in Fig. 4. In addition to the large values of optical deformation potentials, another reason for this effect is that the phonon population and the vibration amplitude corresponding to soft TO modes increase. Furthermore, lowering the TO
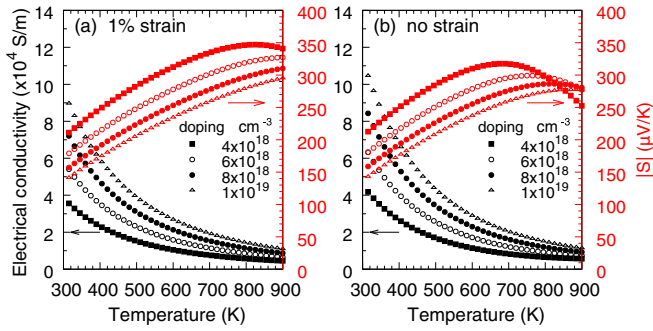
FIG. 5. Electrical conductivity and absolute Seebeck coefficient $|S|$ as a function of temperature for PbTe: (a) with 1% strain and (b) without strain, for the doping concentrations of 4×10^{18}, 6×10^{18}, 8×10^{18}, and 1×10^{19} cm^{-3}.

mode frequency near the zone center means that the energy and momentum conservation conditions for scattering become easier to satisfy, hence increasing the electron–TO-phonon scattering phase space. The energy dependence of the TO scattering rates also changes significantly with lattice expansion, exhibiting a more acousticlike energy dependence close to the phase transition; see Fig. 4. As a result, the TO scattering rates near the phase transition are considerably higher for low-energy electrons close to the conduction band edge than for those at equilibrium.

Longitudinal optical and acoustic phonon scattering is much less sensitive to strain compared with soft modes. LO scattering is dominated by the polar Fröhlich contribution. Even though the changes in optical deformation potentials increase the nonpolar contribution to LO scattering, this increase is small compared with the polar contribution. Most importantly, within the energy range relevant for electronic transport properties, polar LO phonon scattering is still stronger than that of acoustic and TO phonons even for 1% strain. Due to this predominant role of polar LO phonon scattering, strain has a weak influence on the total e-ph scattering in PbTe.

D. Electronic thermoelectric properties

To elucidate the effect of the soft-mode phase transition on electronic transport in PbTe, we illustrate the temperature dependence of the electrical conductivity and the Seebeck coefficient at different doping levels for PbTe with no strain and 1% of strain in Fig. 5. Increasing the lattice constant results in a wider electronic band gap (Fig. 1). This reduces the minority carrier concentration and the bipolar effect that causes a small drop in the Seebeck coefficient at high temperatures and low doping concentrations [21]. Therefore strain leads to an improvement of the Seebeck coefficient above 600 K. A larger band gap due to strain also flattens the conduction band and leads to larger effective masses at the band edge, which explains the higher peak value of the Seebeck coefficient closer to the phase transition. On the other hand, due to larger effective masses, the electrical conductivity is slightly reduced with lattice expansion. In addition, we note that the contribution of ionized impurity scattering to the total electron scattering rates is much smaller than that of phonons

at room temperature and above in PbTe with no strain [18]. When TO modes soften, the static dielectric constant increases (see Table I), thus leading to a reduction in ionized impurity scattering and a negligible effect on electronic transport.

To further understand the role played by the closeness to the phase transition in the electronic thermoelectric transport properties of PbTe, in Figs. 6 and 7 we plot all the relevant properties at 300 and 600 K, respectively, as a function of the doping concentration for different values of $\omega_{\mathrm{TO}}^{\Gamma}$, which correspond to different values of strain indicated in Fig. 3. The electrical conductivity and the electronic contribution to the thermal conductivity are weakly influenced by the proximity to the phase transition for the doping concentrations lower than 1×10^{20} cm^{-3}, even though TO phonon scattering increases in magnitude. The absolute value of the Seebeck coefficient practically does not change with $\omega_{\mathrm{TO}}^{\Gamma}$ at 300 K, while it increases with decreasing $\omega_{\mathrm{TO}}^{\Gamma}$ for low doping concentrations at 600 K. The latter is a consequence of the wider band gap induced by strain, which reduces the bipolar contribution from the hole carriers. The thermoelectric power factor decreases slightly in the peak value closer to the phase transition, since the electrical conductivity is lower compared with equilibrium. Therefore driving PbTe closer to the phase transition via lattice expansion does not appreciably degrade the electronic thermoelectric properties.

E. Discussion

In this paper, we calculate the phonon frequencies and e-ph matrix elements that determine electronic thermoelectric transport using DFPT. These calculations show that although the TO frequency changes significantly due to strain, all other parameters characterizing electronic and phonon band structure and e-ph matrix elements that significantly affect electronic transport properties are fairly insensitive to strain (see Table I). This means that even if the TO frequency is renormalized due to anharmonic effects and/or thermal expansion, our results corresponding to such renormalized frequency would still be similar to those reported in Figs. 6 and 7. Those figures clearly show that electronic thermoelectric properties are almost unaffected by the TO frequency for doping concentrations where the power factor peaks.

We also discuss the implications of driving n-type PbTe closer to the soft-mode phase transition on the thermoelectric figure of merit. Previous calculations of the lattice thermal conductivity κ_L of PbTe show that κ_L can be decreased roughly by a factor of 2 if the lattice constant increases by 1% [11]. The κ_L decrease is a result of stronger anharmonicity and larger phase space for scattering of softer TO modes and heat-carrying acoustic modes [6,7,11,12]. This result together with our calculations of the electronic thermoelectric properties near the phase transition suggests that ZT can be substantially increased (roughly doubled) by driving PbTe to the verge of the soft-mode phase transition due to external stress. This effect arises because soft TO modes that cause low κ_L in PbTe are not the dominant e-ph scattering channel. Polar LO phonon scattering is the strongest scattering mechanism and is fairly constant towards the phase transition. This specific feature of the e-ph interaction in PbTe allows the soft-mode phase transition to effectively increase
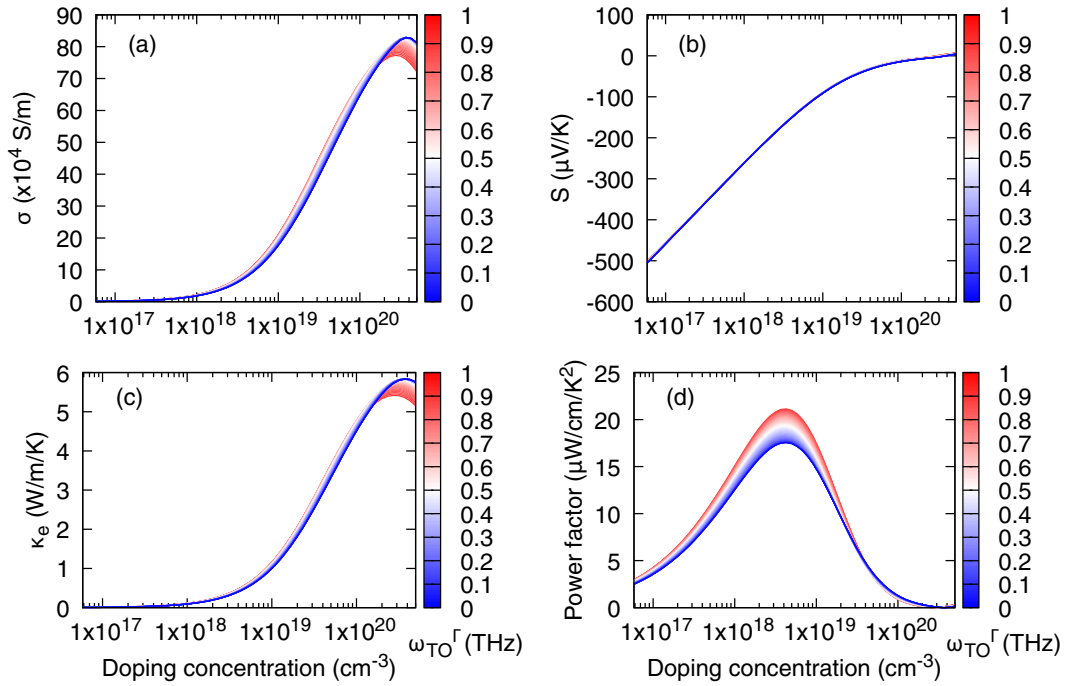
FIG. 6. Thermoelectric transport properties as a function of doping concentration at 300 K for different transverse optical (TO) phonon frequencies at the zone center obtained by applying strain: (a) electrical conductivity σ, (b) Seebeck coefficient $|S|$, (c) electronic thermal conductivity κ_e, and (d) power factor σS^2.

scattering of heat-carrying acoustic phonons while preserving the electronic thermoelectric properties, hence materializing the "phonon-glass–electron-crystal" idea without nanostructuring or alloying.

IV. CONCLUSION

Using first-principles calculations, we investigate electronic thermoelectric transport in *n*-type PbTe driven closer to its intrinsic soft-mode phase transition via lattice
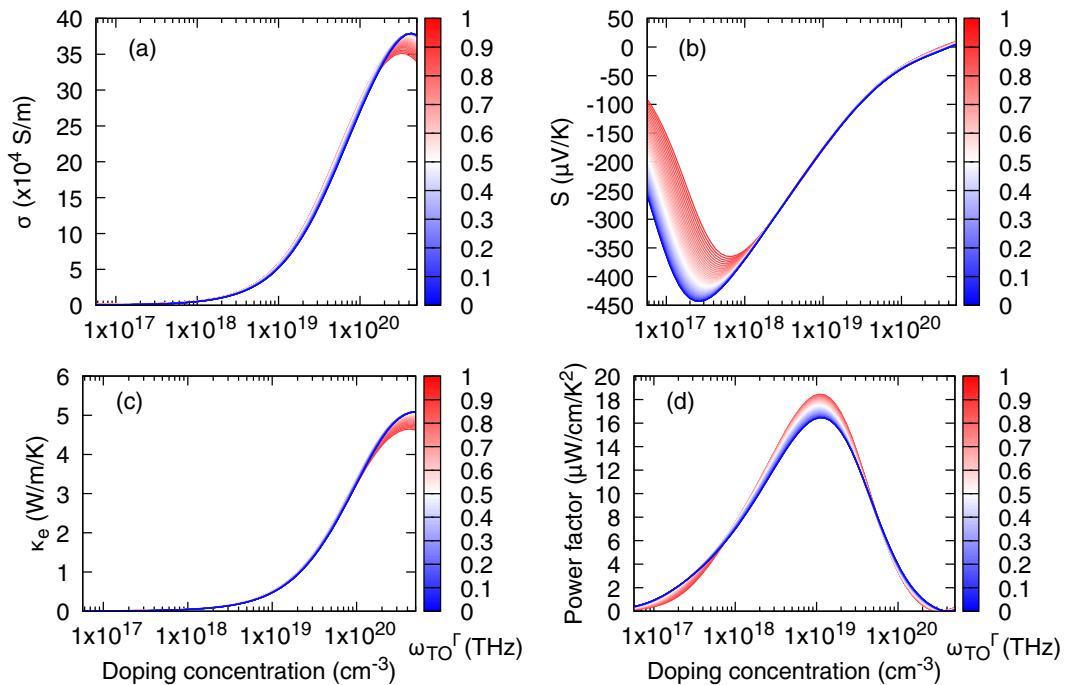

FIG. 7. Thermoelectric transport properties as a function of doping concentration at 600 K for different transverse optical (TO) phonon frequencies at the zone center obtained by applying strain: (a) electrical conductivity σ, (b) Seebeck coefficient $|S|$, (c) electronic thermal conductivity κ_e, and (d) power factor σS^2.

expansion due to external stress. We find that even though soft transverse optical modes interact more strongly with electrons responsible for transport when PbTe approaches the phase transition, soft-mode scattering is relatively weak compared with longitudinal optical mode scattering in contrast to SrTiO$_3$ [20]. The dominant electron–longitudinal-optical-phonon interaction and the electronic thermoelectric properties are fairly insensitive to the proximity to the phase transition. Consequently, the thermoelectric figure of merit ZT of n-type PbTe can be enhanced by increasing the proximity to the soft-mode phase transition via lattice expansion since the lattice thermal conductivity can be sizably reduced [11]. A few well-known high-performance thermoelectric materials, such as GeTe and

SnTe, undergo the same type of soft-mode phase transition with temperature. Our work suggests new opportunities to further improve the ZT values of these materials.

ACKNOWLEDGMENTS

[1] G. J. Snyder and E. S. Toberer, Nat. Mater. **7**, 105 (2008).

[2] J. He and T. M. Tritt, Science **357**, eaak9997 (2017).

[3] X. Zhou, Y. Yan, X. Lu, H. Zhu, X. Han, G. Chen, and Z. Ren, Mater. Today **21**, 974 (2018).

[4] M. Beekman, D. T. Morelli, and G. S. Nolas, Nat. Mater. **14**, 1182 (2015).

[5] T. Takabatake, K. Suekuni, T. Nakayama, and E. Kaneshita, Rev. Mod. Phys. **86**, 669 (2014).

[6] O. Delaire, J. Ma, K. Marty, A. F. May, M. A. McGuire, M.-H. Du, D. J. Singh, A. Podlesnyak, G. Ehlers, M. D. Lumsden, and B. C. Sales, Nat. Mater. **10**, 614 (2011).

[7] T. Shiga, J. Shiomi, J. Ma, O. Delaire, T. Radzynski, A. Lusakowski, K. Esfarjani, and G. Chen, Phys. Rev. B **85**, 155203 (2012).

[8] C. W. Li, O. Hellman, J. Ma, A. F. May, H. B. Cao, X. Chen, A. D. Christianson, G. Ehlers, D. J. Singh, B. C. Sales, and O. Delaire, Phys. Rev. Lett. **112**, 175501 (2014).

[9] C. W. Li, J. Hong, A. F. May, D. Bansal, S. Chi, T. Hong, G. Ehlers, and O. Delaire, Nat. Phys. **11**, 1063 (2015).

[10] L.-D. Zhao, S.-H. Lo, Y. Zhang, H. Sun, G. Tan, C. Uher, C. Wolverton, V. P. Dravid, and M. G. Kanatzidis, Nature (London) **508**, 373 (2014).

[11] A. H. Romero, E. K. U. Gross, M. J. Verstraete, and O. Hellman, Phys. Rev. B **91**, 214310 (2015).

[12] R. M. Murphy, É. D. Murray, S. Fahy, and I. Savić, Phys. Rev. B **93**, 104304 (2016).

[13] U. Aseginolaza, R. Bianco, L. Monacelli, L. Paulatto, M. Calandra, F. Mauri, A. Bergara, and I. Errea, Phys. Rev. Lett. **122**, 075901 (2019).

[14] C. Chang, D. Wang, D. He, W. He, F. Zhu, G. Wang, J. He, and L.-D. Zhao, Adv. Energy Mater. **9**, 1901334 (2019).

[15] J. Hong and O. Delaire, Mater. Today Phys. **10**, 100093 (2019).

[16] J. M. Skelton, S. C. Parker, A. Togo, I. Tanaka, and A. Walsh, Phys. Rev. B **89**, 205203 (2014).

[17] R. M. Murphy, É. D. Murray, S. Fahy, and I. Savić, Phys. Rev. B **95**, 144302 (2017).

[18] J. Cao, J. D. Querales-Flores, A. R. Murphy, S. Fahy, and I. Savić, Phys. Rev. B **98**, 205202 (2018).

[19] R. D'Souza, J. Cao, J. D. Querales-Flores, S. Fahy, and I. Savić, Phys. Rev. B **102**, 115204 (2020).

[20] J.-J. Zhou, O. Hellman, and M. Bernardi, Phys. Rev. Lett. **121**, 226603 (2018).

[21] J. Cao, J. Querales-Flores, S. Fahy, and I. Savić, Mater. Today Phys. **12**, 100172 (2020).

[22] S. Poncé, E. Margine, C. Verdi, and F. Giustino, Comput. Phys. Commun. **209**, 116 (2016).

[23] X. Gonze and C. Lee, Phys. Rev. B **55**, 10355 (1997).

[24] S. Baroni, S. de Gironcoli, A. Dal Corso, and P. Giannozzi, Rev. Mod. Phys. **73**, 515 (2001).

[25] P. Giannozzi, S. Baroni, N. Bonini, M. Calandra, R. Car, C. Cavazzoni, D. Ceresoli, G. L. Chiarotti, M. Cococcioni, I. Dabo, A. Dal Corso, S. de Gironcoli, S. Fabris, G. Fratesi, R. Gebauer, U. Gerstmann, C. Gougoussis, A. Kokalj, M. Lazzeri, L. Martin-Samos *et al.*, J. Phys.: Condens. Matter **21**, 395502 (2009).

[26] P. Giannozzi, O. Andreussi, T. Brumme, O. Bunau, M. B. Nardelli, M. Calandra, R. Car, C. Cavazzoni, D. Ceresoli, M. Cococcioni, N. Colonna, I. Carnimeo, A. D. Corso, S. de Gironcoli, P. Delugas, R. A. DiStasio Jr, A. Ferretti, A. Floris, G. Fratesi, G. Fugallo *et al.*, J. Phys.: Condens. Matter **29**, 465901 (2017).

[27] J. Heyd, G. E. Scuseria, and M. Ernzerhof, J. Chem. Phys. **118**, 8207 (2003).

[28] J. Heyd and G. E. Scuseria, J. Chem. Phys. **121**, 1187 (2004).

[29] G. Kresse and J. Furthmüller, Comput. Mat. Sci. **6**, 15 (1996).

[30] G. Kresse and D. Joubert, Phys. Rev. B **59**, 1758 (1999).

[31] P. B. Allen and V. Heine, J. Phys. C: Solid State Phys. **9**, 2305 (1976).

[32] P. B. Allen and M. Cardona, Phys. Rev. B **23**, 1495 (1981).

[33] P. B. Allen and M. Cardona, Phys. Rev. B **27**, 4760 (1983).

[34] S. Poncé, Y. Gillet, J. L. Janssen, A. Marini, M. Verstraete, and X. Gonze, J. Chem. Phys. **143**, 102813 (2015).

[35] J. D. Querales-Flores, J. Cao, S. Fahy, and I. Savić, Phys. Rev. Mater. **3**, 055405 (2019).

[36] M. S. Dresselhaus, G. Dresselhaus, and A. Jorio, *Group Theory: Application to the Physics of Condensed Matter*, 1st ed. (Springer, Berlin, 2008), pp. 97, 246, 254–255.

[37] A. R. Murphy, F. Murphy-Armando, S. Fahy, and I. Savić, Phys. Rev. B **98**, 085201 (2018).

[38] F. Giustino, M. L. Cohen, and S. G. Louie, Phys. Rev. B **76**, 165108 (2007).

[39] A. A. Mostofi, J. R. Yates, G. Pizzi, Y.-S. Lee, I. Souza, D. Vanderbilt, and N. Marzari, Comput. Phys. Commun. **185**, 2309 (2014).

[40] F. Murphy-Armando and S. Fahy, Phys. Rev. B **78**, 035202 (2008).

[41] C. Herring and E. Vogt, Phys. Rev. **101**, 944 (1956).

[42] B. K. Ridley, "*Quantum Processes in Semiconductors*" (Oxford University Press, Oxford, 1999), pp. 143–144.

[43] I. I. Ravich, *Semiconducting Lead Chalcogenides*, Vol. 5 (Springer, New York, 2013).

[44] M. P. Jiang, M. Trigo, I. Savić, S. Fahy, É. D. Murray, C. Bray, J. Clark, T. Henighan, M. Kozina, M. Chollet, J. M. Glownia, M. C. Hoffmann, D. Zhu, O. Delaire, A. F. May, B. C. Sales, A. M. Lindenberg, P. Zalden, T. Sato, R. Merlin *et al.*, Nat. Commun. **7**, 12291 (2016).

[45] R. H. Lyddane, R. G. Sachs, and E. Teller, Phys. Rev. **59**, 673 (1941).